

Supporting Information

Long-Persistent Luminescence by Host-Guest

Förster Resonance Energy Transfer

*Hui-Li Sun, Qiang-Sheng Zhang, Zhong-Hao Wang, Yan-Ting Huang, and Mei Pan**

H.-L. Sun, Z.-H. Wang, Y.-T. Huang, Prof. M. Pan

MOE Laboratory of Bioinorganic and Synthetic Chemistry,

Lehn Institute of Functional Materials,

IGCME, GBRCE for Functional Molecular Engineering,

School of Chemistry, Sun Yat-Sen University Guangzhou 510006, P. R. China

E-mail: panm@mail.sysu.edu.cn

Dr. Q.-S. Zhang

Hainan Provincial Key Laboratory of Fine Chem,

School of Chemistry and Chemical Engineering,

Hainan University

Haikou 570228, P. R. China.cn

1. Experimental Section

Materials and Instrumentations

All reaction materials were obtained from commercial suppliers and used without further purification. IR spectra were recorded using Nicolet/Nexus-670 FT-IR spectrometer in the region of 4000-400 cm^{-1} using KBr pellets. A Mini-Pellet Press of Specac is used to compress the samples. The single-crystal structures were determined by the Rigaku X-ray single-crystal diffraction system SuperNova with monochromator Cu-K α radiation ($\lambda = 1.54184 \text{ \AA}$). NMR spectra were recorded on a JEOL EX270 spectrometer (^1H : 400 MHz; ^{13}C : 100 MHz). UV-Visible absorption spectra were recorded using a Shimadzu UV-2450 spectrophotometer. Fluorescence spectra and decay lifetimes were measured by Edinburgh FLS 1000 spectrometer. The emission quantum yields were measured on a Hamamatsu C9920-02G absolute PL quantum yield measurement system.

X-ray single crystal structural analysis

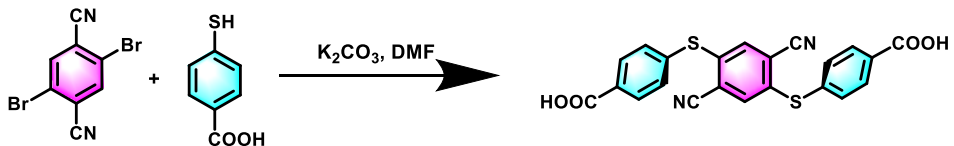
Single-crystal X-ray diffraction data for **DPSD** and **DPOD** were collected on a Rigaku Oxford SuperNova X-RAY diffractometer system equipped with a Cu sealed tube ($\lambda = 1.54178 \text{ \AA}$) at 50 kV and 0.80 mA. The structure was solved by direct methods, and refined by full-matrix least-square methods with the SHELXL-2014 program package.^[1] All hydrogen atoms were located in calculated positions and refined anisotropically. The crystallographic data for **DPSD** and **DPOD** were listed in Table S1. The single crystal data have been deposited in the Cambridge Crystallographic Data Center (CCDC No: 2312419, 2312421). The data can be obtained free of charge from The Cambridge Crystallographic Data Centre (**α -Cellulose**: (CCDC No : 810597)).

Calculation methods

Simulation calculations of **DPSD+ α -Cellulose** and **DPOD+ α -Cellulose**, **DPSD** and **DPOD**, were carried out with Gaussian 09 program package.^[2] **DPSD+ α -Cellulose** and **DPOD+ α -Cellulose**, **DPSD** and **DPOD** at the level of CAM-B3LYP-GD3(BJ)/6-311G** have been evaluated. Time-dependent density functional theory (TD-DFT) calculations were performed based on the optimized molecular structure. The frontier molecular orbitals (FMOs) analysis were carried out by Multiwfn program^[3-4]. All orbitals were visualized by VMD (isovalue = 0.02).^[5]

Synthesis of the DPSD

The synthesis of 4,4'-(2,5-dicyano-1,4-phenylene)bis(sulfanediyl)dibenzoic acid (**DPSD**).^[6] 2,5-dibromophtalonitrile (100 mg, 0.35 mmol), 4-mercaptopbenzoic acid (162 mg, 1.05 mmol) and potassium carbonate (290 mg, 2.1 mmol) were added under nitrogen into a 100 mL round bottom flask followed by the addition of dry DMF (10 mL). The solution was stirred at 50 °C for 24 h. Then the reaction was quenched very carefully with 4 M HCl (30 mL), the product precipitated as lightly green solid. This solid was separated by filtration and washed with distilled water. The product recrystallized in DMF and was dried under vacuum. (Yield 150 mg, 57%). Molecular formula: C₂₂H₁₂N₂O₄S₂. ¹H NMR (400 MHz, DMSO-*d*₆): δ (ppm) 13.11 (s, 2H), 8.08 (d, 4H, J = 8.5 Hz), 7.96 (s, 2H), 7.52 (d, 4H, J = 12 Hz); ¹³C NMR (100 MHz, DMSO-*d*₆): δ (ppm) 167.07, 138.70, 138.37, 138.11, 137.83, 131.13, 131.07, 119.55, 115.55. IR (KBr, cm⁻¹): 3428(m), 3091 (w), 2994 (w), 2820 (w), 2663 (w), 2555(w), 2233(w), 2026(w), 1694 (s), 1586 (s), 1388 (s), 1288 (s), 1172 (w), 1123 (w), 1016 (w), 941 (w), 866 (w), 808 (w), 758(w), 692(w), 643(w), 560(w).



Synthesis of the DPOD

The synthesis of 4,4'-(2,5-dicyano-1,4-phenylene)bis(oxy)dibenzoic acid (**DPOD**). Tetrachloroterephthalonitrile (200.00 mg, 0.75 mmol), 4-hydroxybenzoic acid (616.5 mg, 4.5 mmol) and potassium carbonate (1.66 g, 12 mmol) were added under nitrogen into a 100 mL round bottom flask followed by the addition of dry DMF (10 mL). The solution was stirred at 80 °C for 48 h. Then the reaction was quenched very carefully with 4 M HCl (30 mL), the product precipitated as white solid. This solid was separated by filtration and washed with distilled water. The product recrystallized in ethanol and was dried under vacuum. (Yield 194.0 mg, 45%). Molecular formula: C₂₂H₁₂N₂O₆. ¹H NMR (400 MHz, DMSO-*d*₆): δ (ppm) 12.95 (s, 2H), 8.04 (d, 4H, J = 8.0 Hz), 8.00 (s, 2H), 7.30 (d, 4H, J = 12.0 Hz); ¹³C NMR (100 MHz, DMSO-*d*₆): δ (ppm) 167.06, 159.66, 153.52, 132.34, 127.79, 126.16, 118.44, 114.27, 111.00. IR (KBr, cm⁻¹): ν = 3428 (m), 2810 (w), 2553 (w), 2236 (w), 2027 (w), 1689 (s), 1603 (s), 1490 (m), 1399 (m), 1346 (m), 1281 (m), 1227 (m), 1168 (m), 1013 (m), 888 (m), 846 (m), 765 (m), 690 (w), 658 (w), 545 (w), 492 (w).

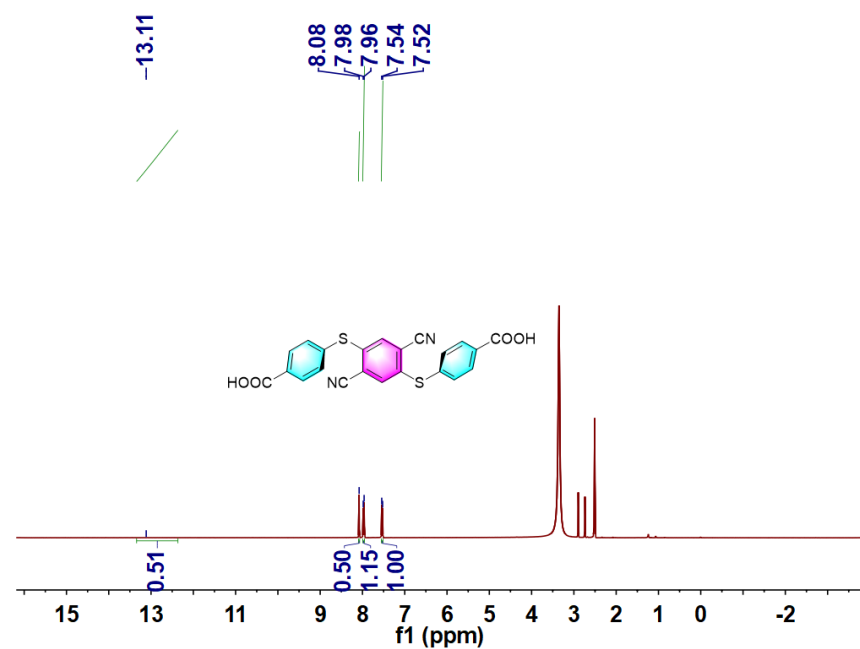


Figure S1. ^1H NMR spectrum of DPSD in $\text{DMSO}-d_6$.

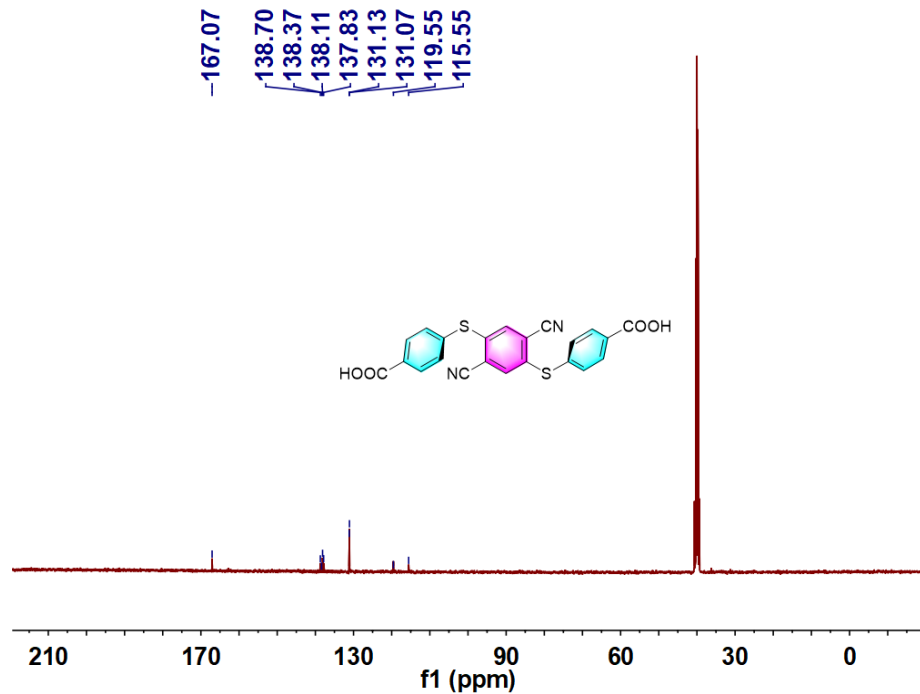


Figure S2. ^{13}C NMR spectrum of DPSD in $\text{DMSO}-d_6$.

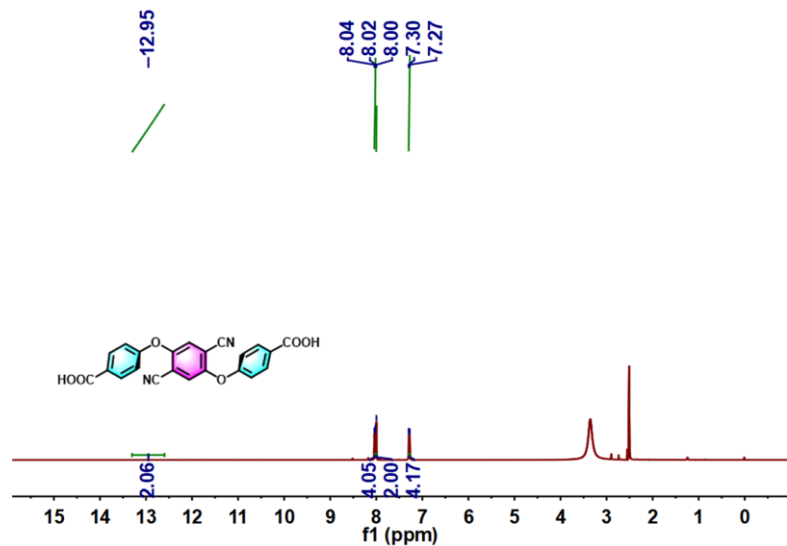


Figure S3. ^1H NMR spectrum of **DPOD** in $\text{DMSO}-d_6$.

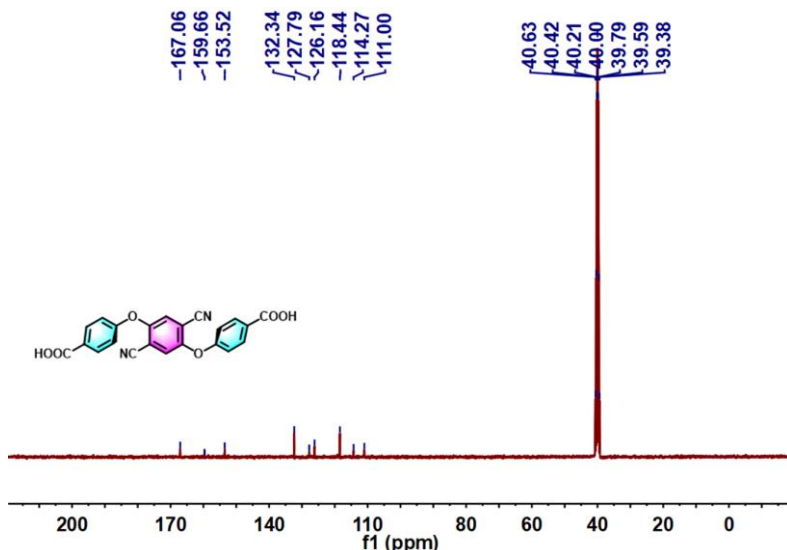


Figure S4. ^{13}C NMR spectrum of **DPOD** in $\text{DMSO}-d_6$.

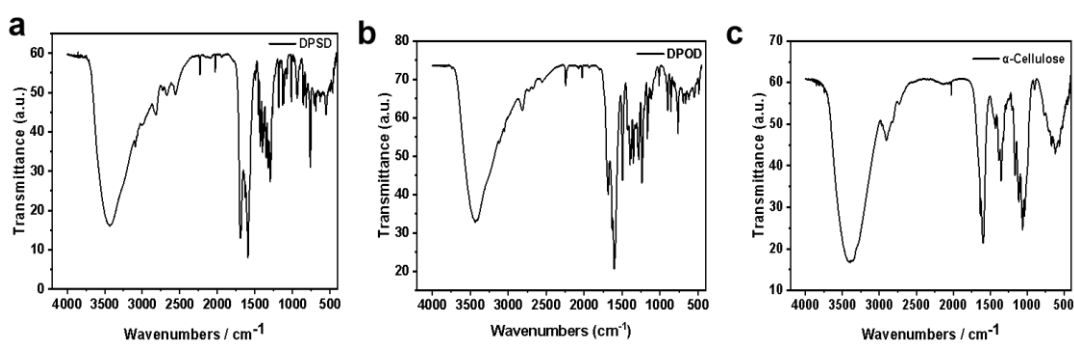


Figure S5. FT-IR spectra of (a) DPSD, (b) DPOD and (c) α -Cellulose.

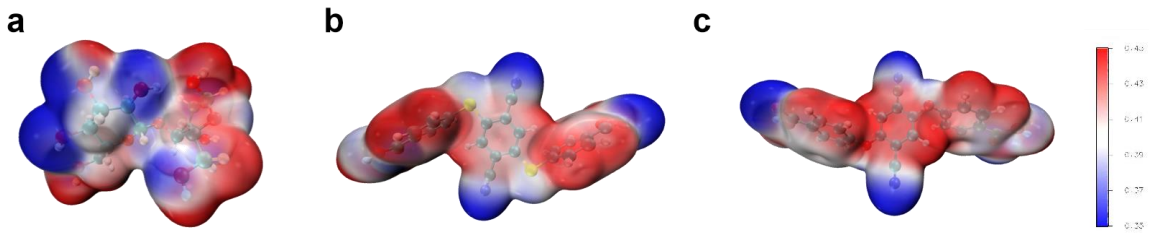


Figure S6. The electrostatic potential (ESP) surfaces of (a) α -Cellulose, (b) DPSD and (c) DPOD.

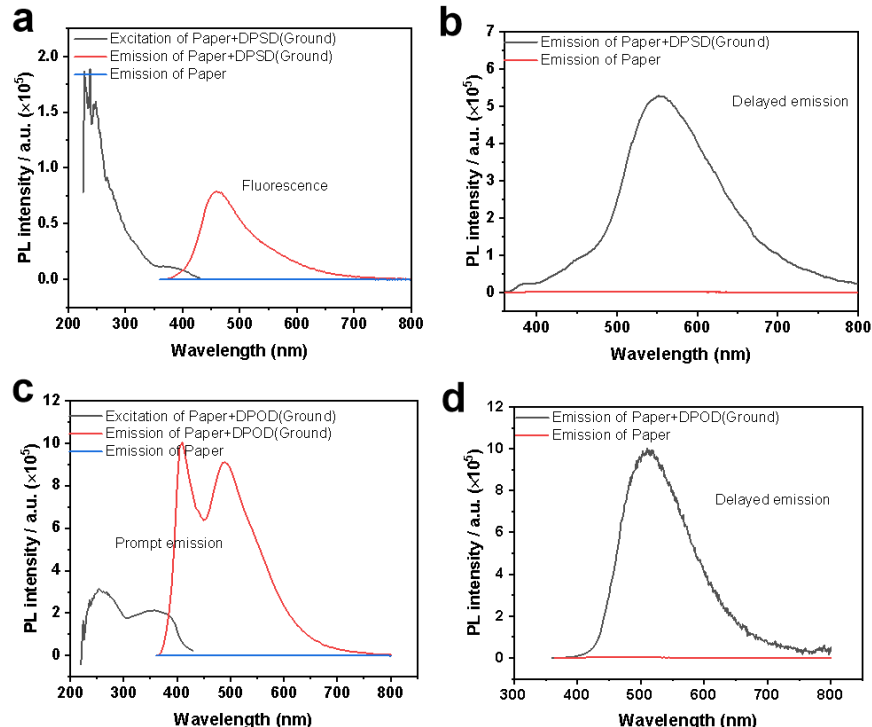
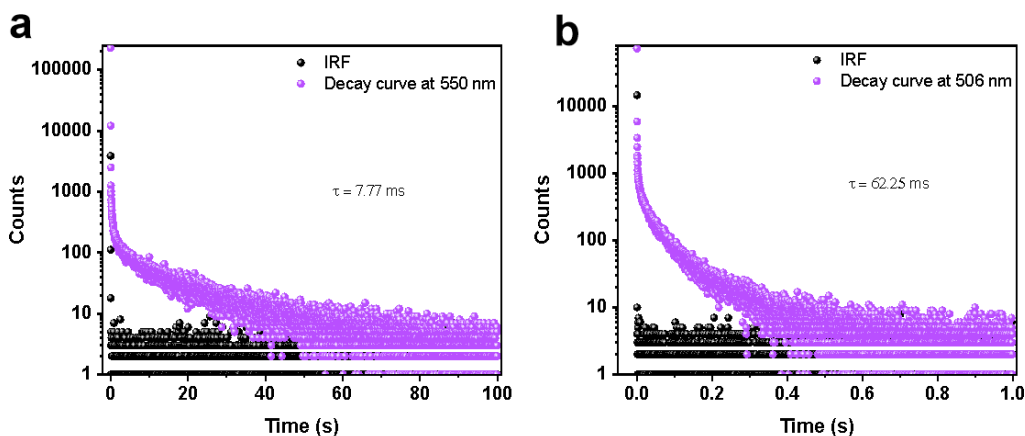


Figure S7. Prompt excitation and emission spectra of paper, paper+DPSD (a), paper+DPOD (c) and delayed emission spectra of paper, paper+DPSD (b), paper+DPOD (d) under 340 nm excitation.



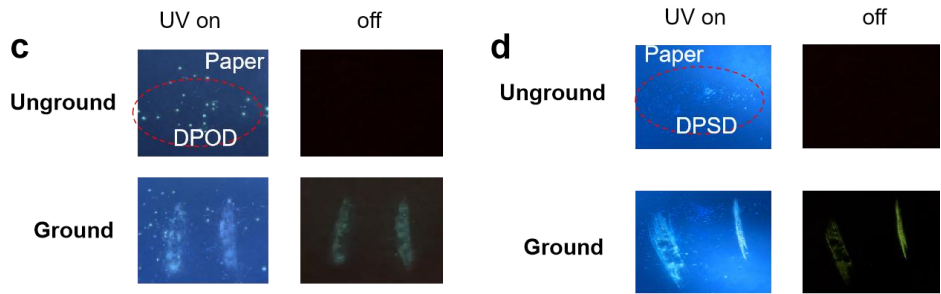


Figure S8. Decay curves of **paper+DPsd** at 550 nm (a) and **paper+DPOD** at 506 nm (b) under 340 nm excitation; (c) Place **DPOD** and (d) **DPsd** on filter paper, grinding the sample on the paper, and recording the photographs before and after grinding, respectively.

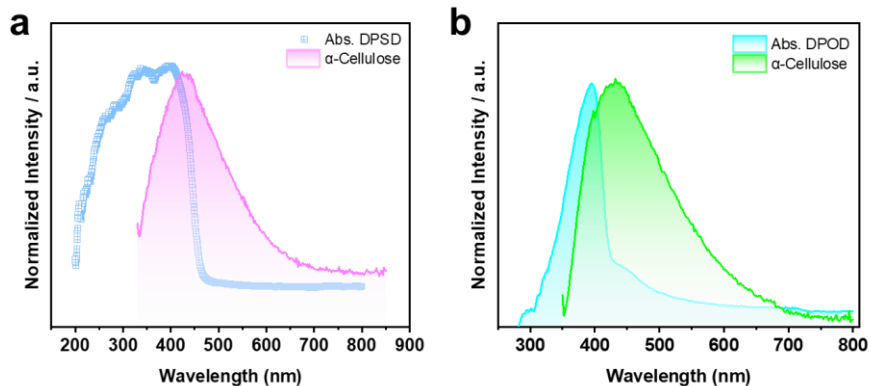


Figure S9. (a) PL spectrum (red curve) of donor (**α -Cellulose**) under 340 nm excitation and UV-visible absorption spectrum of acceptor (**DPsd**) (blue curve); (b) PL spectrum (green curve) of donor (**α -Cellulose**) under 340 nm excitation and UV-visible absorption spectrum of acceptor (**DPOD**) (blue curve).

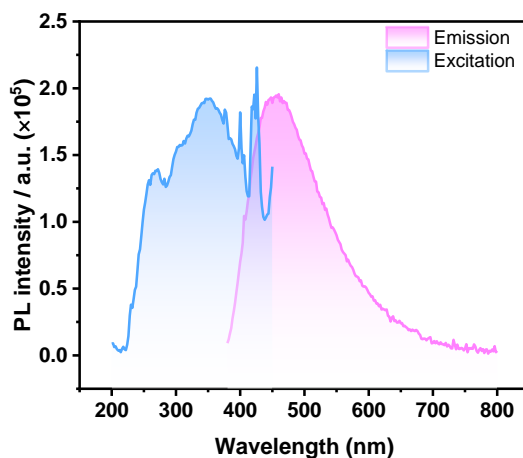


Figure S10. The excitation and emission spectra of **α -Cellulose** under 340 nm excitation.

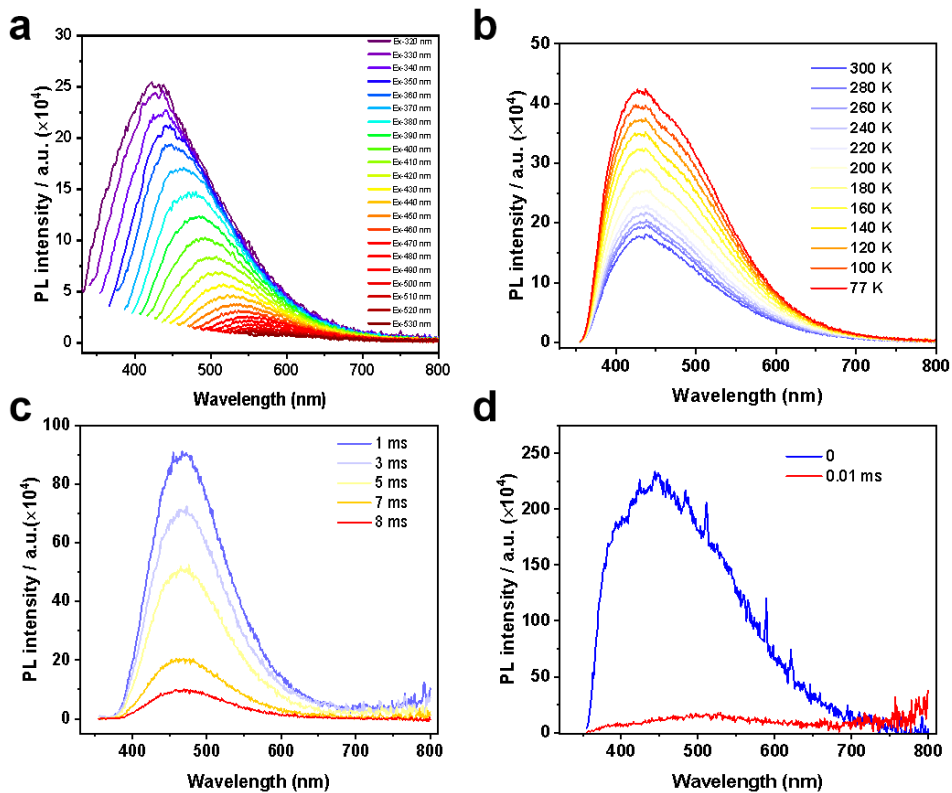


Figure S11. (a) The emission spectra of α -Cellulose under different excitations; (b) Temperature-dependent steady-state PL spectra of α -Cellulose from 77 K–300 K under 340 nm excitation; PL spectra of α -Cellulose measured at different time intervals and different temperature of 77 K (c) and 300 K (d) after the removal of 340 nm UV light.

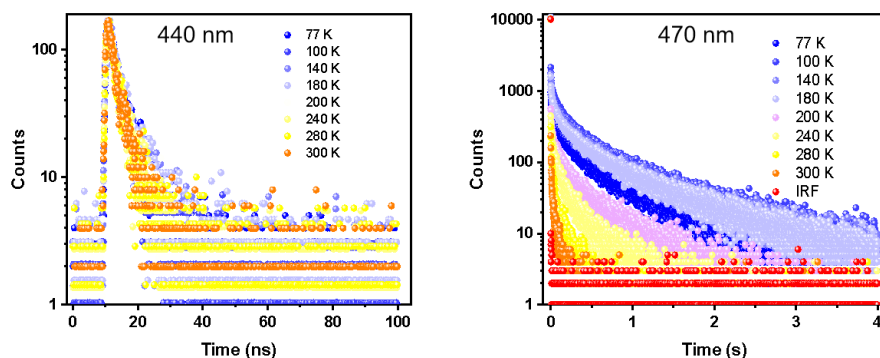


Figure S12. Decay curves of α -Cellulose at 440 nm (a) and at 470 nm (b) from 77 K–300 K (b) under 340 nm excitation.

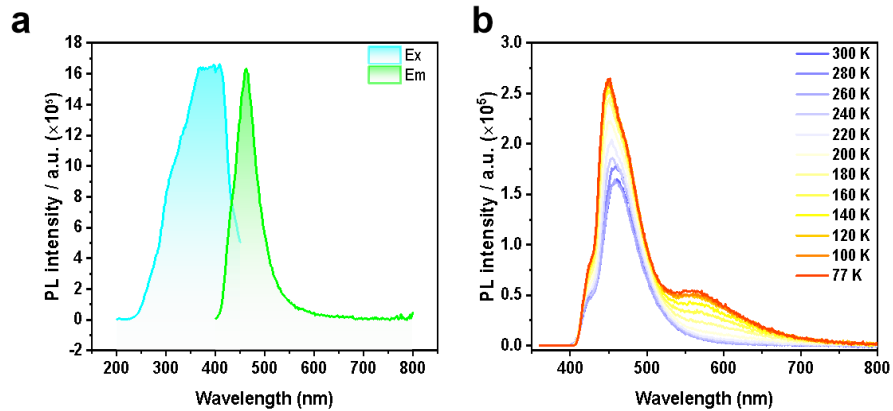


Figure S13. (a) The excitation and emission spectra of **DPSD**; (b) Temperature-dependent steady-state PL spectra of **DPSD** from 77 K–300 K.

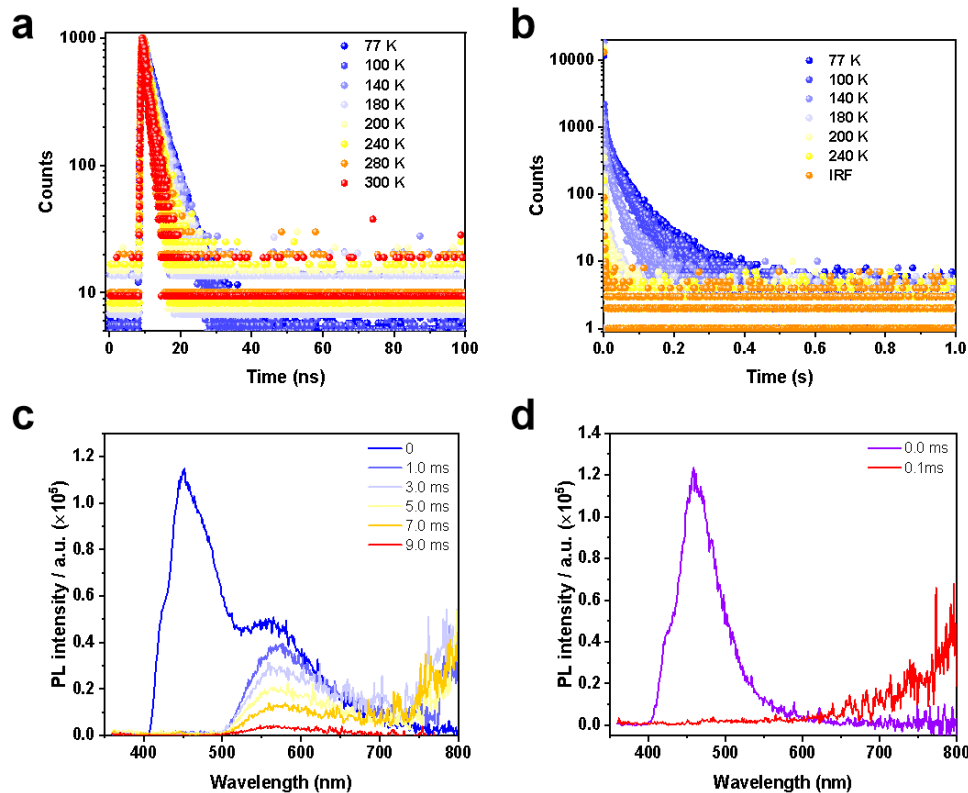


Figure S14. Decay curves of **DPSD** at 455 nm from 77 K–300 K (a) and at 570 nm from 77 K–240 K (b); PL spectra of **DPSD** measured at different time intervals and different temperature of 77 K (c) and 300 K (d).

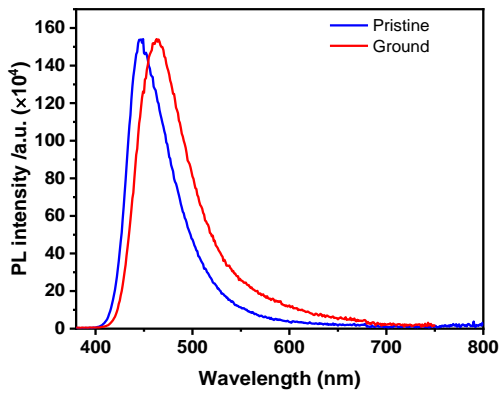


Figure S15. Emission spectra of DPSD before and after grinding.

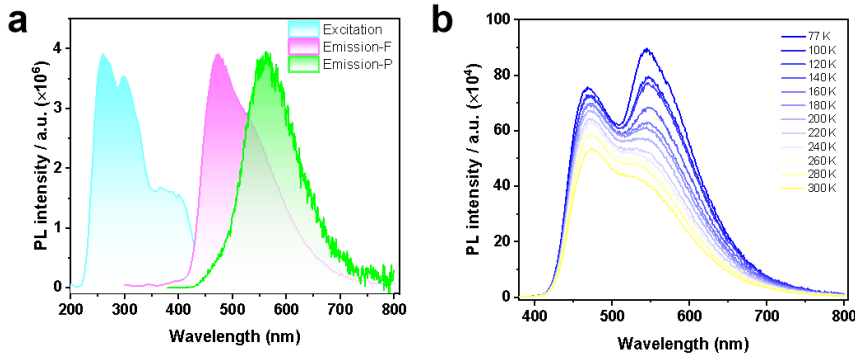


Figure S16. (a) The excitation and emission spectra of α -Cellulose+DPSD (mass ratio=100:1); (b) Temperature-dependent steady-state PL spectra of α -Cellulose+DPSD from 77 K–300 K.

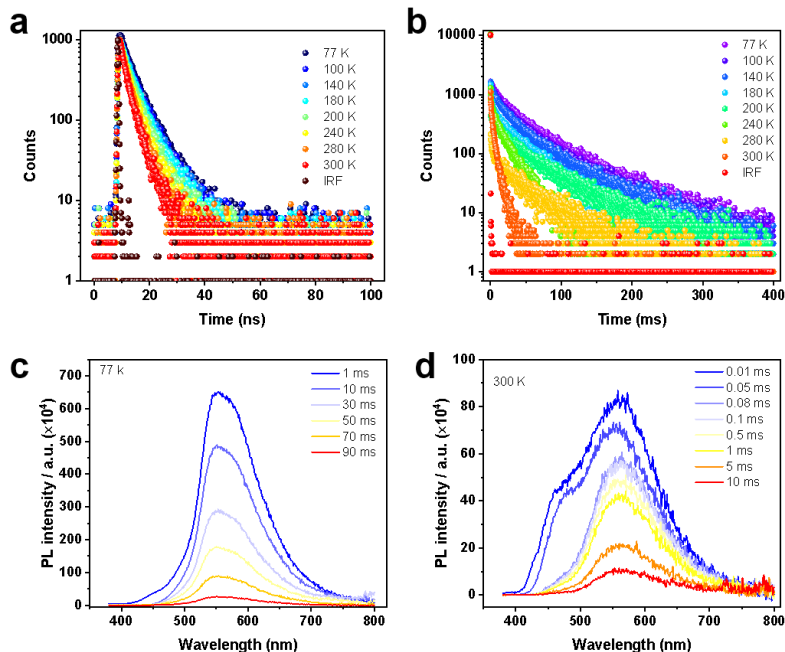


Figure S17. Decay curves of α -Cellulose+DPSD at 470 nm (a) and at 554 nm from 77 K–300 K (b); PL spectra of α -Cellulose+DPSD measured at different time intervals and

different temperature of 77 K (c) and 300 K (d) after the removal of 340 nm UV light.

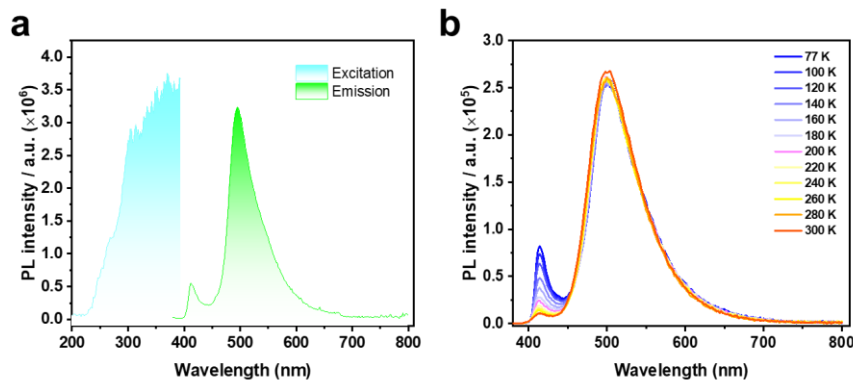


Figure S18. (a) The excitation and emission spectra of **DPOD**; (b) Temperature-dependent steady-state PL spectra of **DPOD** from 77 K–300 K.

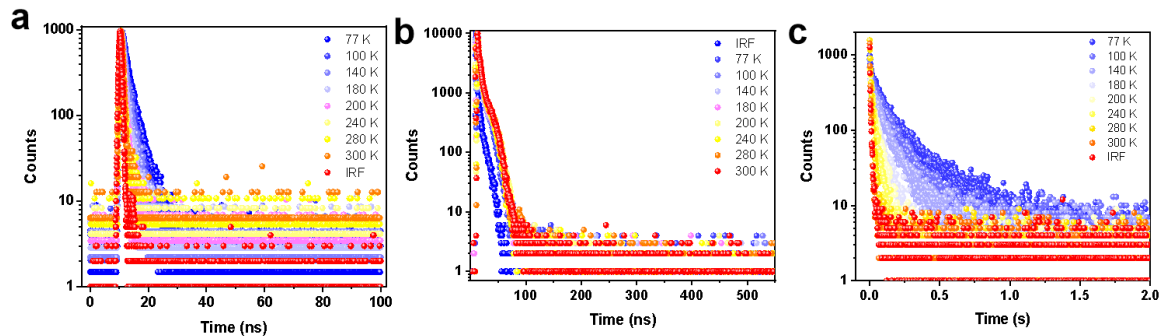


Figure S19. Decay curves of **DPOD** at (a) 417 nm, (b) 500 nm, (c) 575 nm from 77 K–300 K.

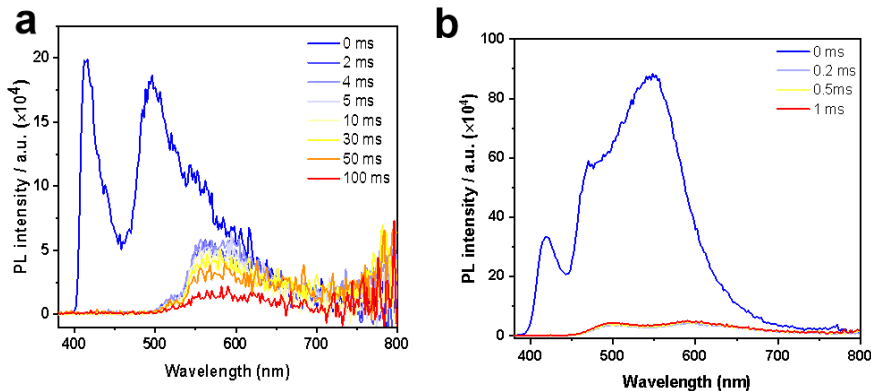


Figure S20. PL spectra of **DPOD** measured at different time intervals and different temperature of 77 K (a) and 300 K (b) after the removal of 340 nm UV light.

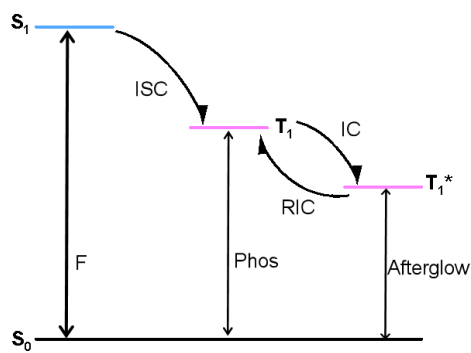


Figure S21. Proposed mechanism of photophysical processes based on ISC of **DPOD** (S, singlet; T, triplet; IC, internal conversion; RIC, reverse internal conversion; F, fluorescence; Phos, phosphorescence).

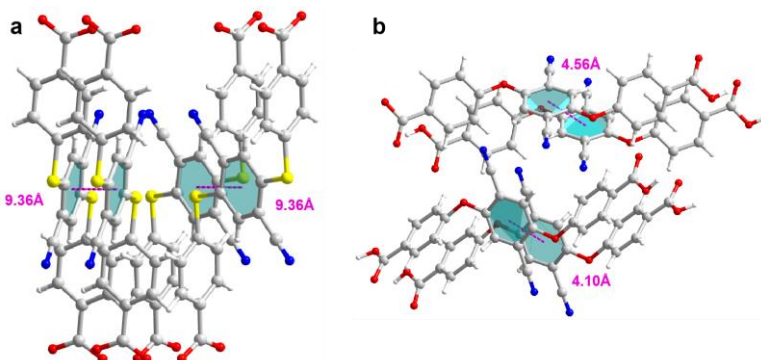


Figure S22. Packing among the (a) **DPSD** and (b) **DPOD** crystal by $\pi \cdots \pi$ interactions.

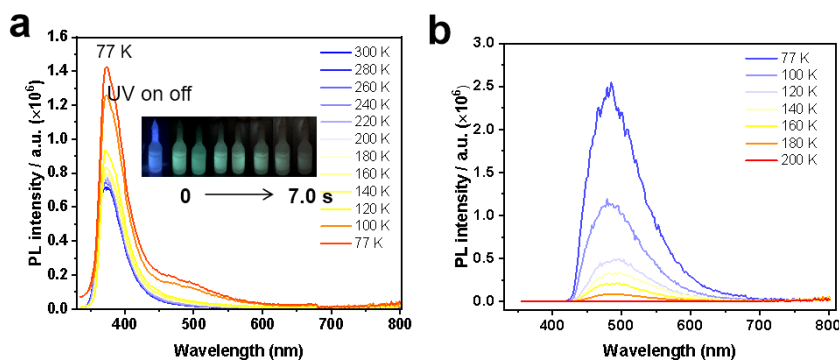


Figure S23. (a) Temperature-dependent steady-state prompt PL spectra of **DPOD** from 77 K–300 K and (b) delayed emission spectra from 77 K–200 K in 2-MTHF (50.0 μ M). The inserts show the photos of **DPOD** in 2-MTHF at 77 K under 365 nm.

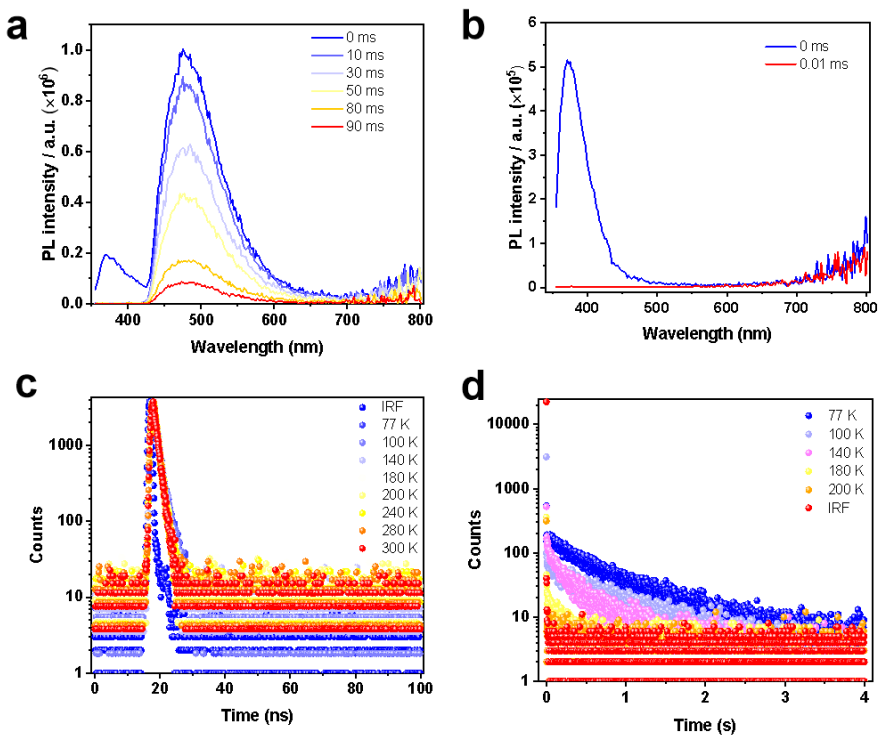


Figure S24. PL spectra of **DPOD** in 2-MTHF (50.0 μM) measured at different time intervals and different temperature of 77 K (a) and 300 K (b); Decay curves of **DPOD** in 2-MTHF at 375 nm from 77 K-300 K (c) and at 486 nm from 77 K-200 K (d).

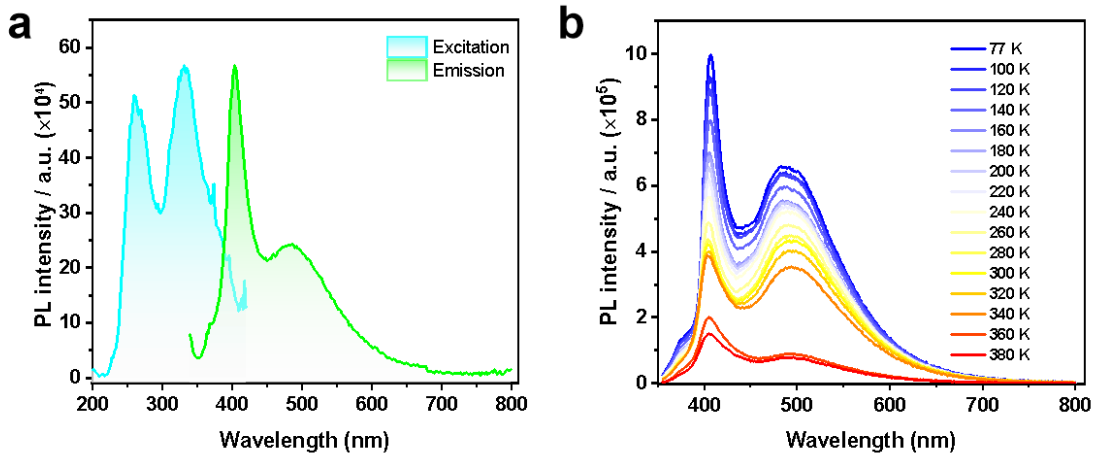


Figure S25. (a) The excitation and emission spectra of **α -Cellulose+DPOD** (mass ratio=100:1); (b) Temperature-dependent steady-state PL spectra of **α -Cellulose+DPOD** from 77 K–380 K.

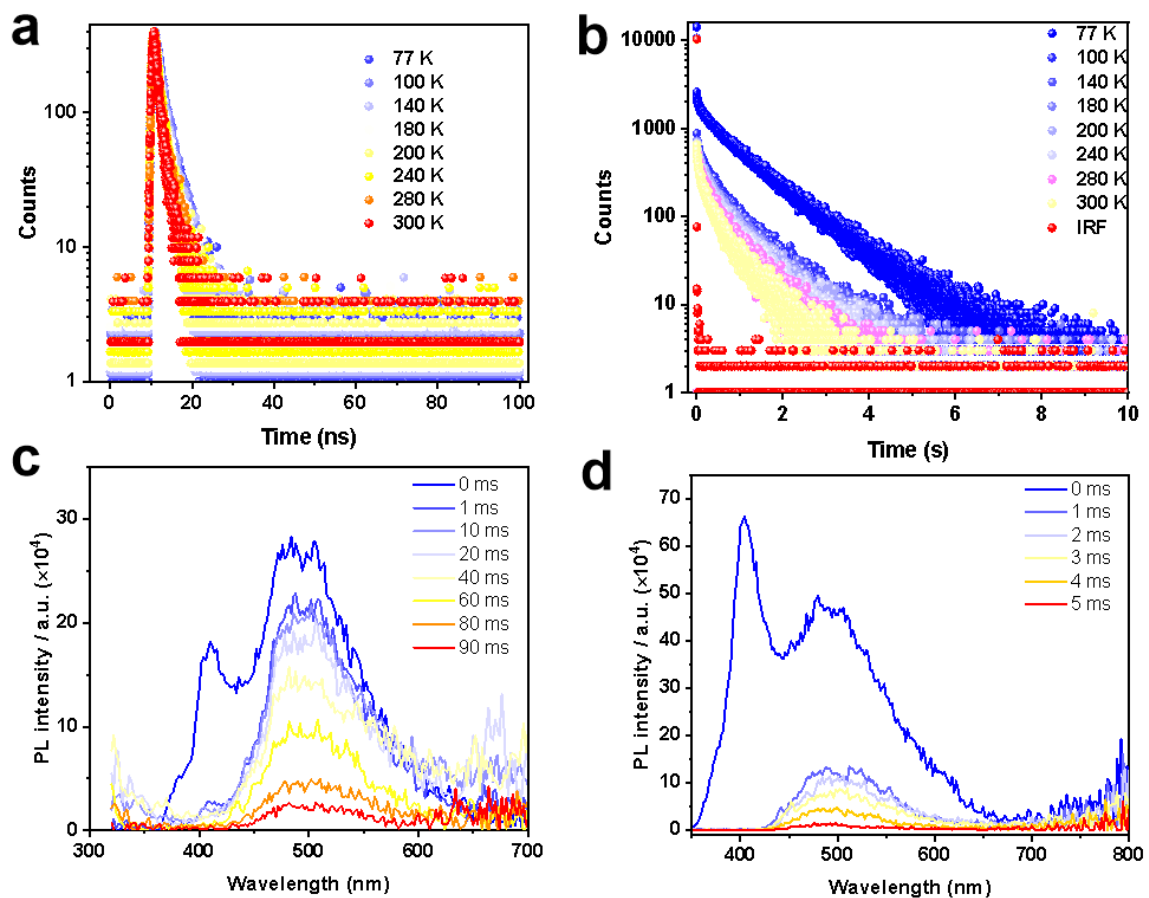


Figure S26. Decay curves of α -Cellulose+DPOD at 417 nm (a) and at 492 nm from 77 K-300 K (b); PL spectra of α -Cellulose+DPOD measured at different time intervals and different temperature of 77 K (c) and 300 K (d) after the removal of 340 nm UV light.

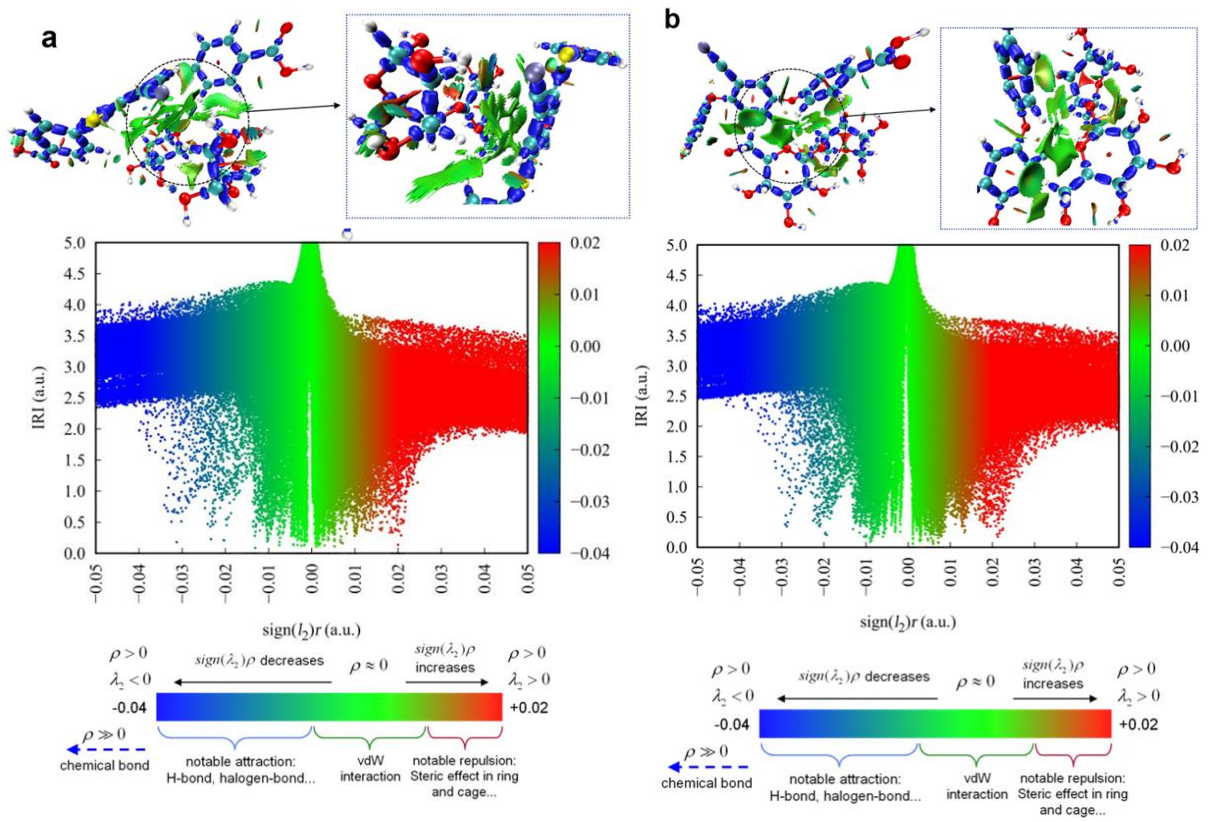


Figure S27. The interaction region indicator (IRI) analysis of (a) α -Cellulose+DPSD, (b) α -Cellulose+DPOD.

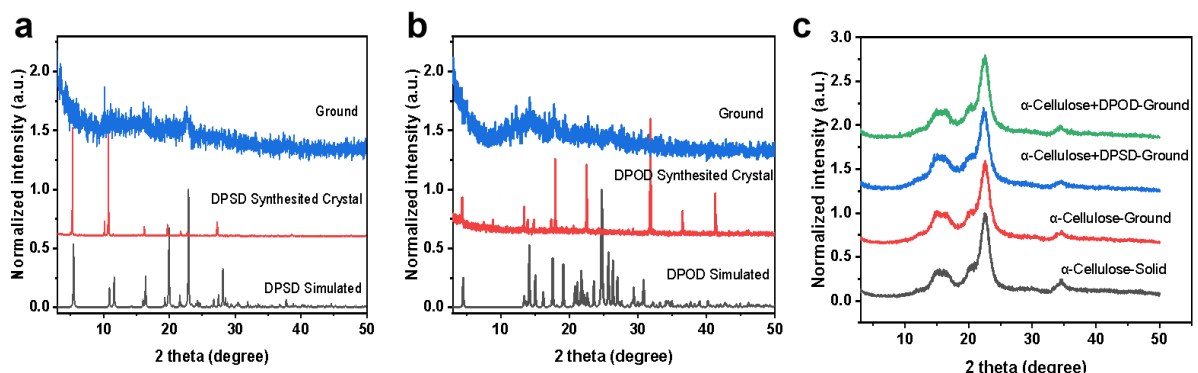


Figure S28. (a) PXRD patterns of DPSD crystal before and after grinding; (b) PXRD patterns of DPOD crystal before and after grinding; (c) PXRD patterns of α -Cellulose before and after grinding, and host-guest doping systems in ground states.

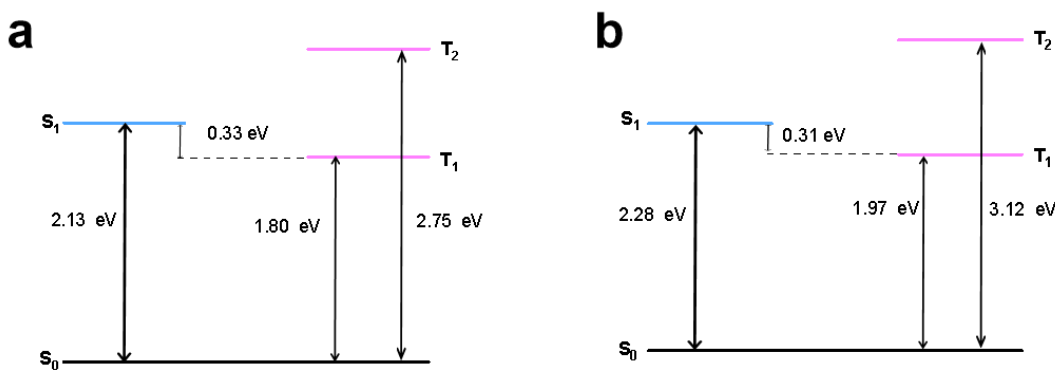


Figure S29. Energy level diagram for α -Cellulose+DPSD and α -Cellulose+DPOD.

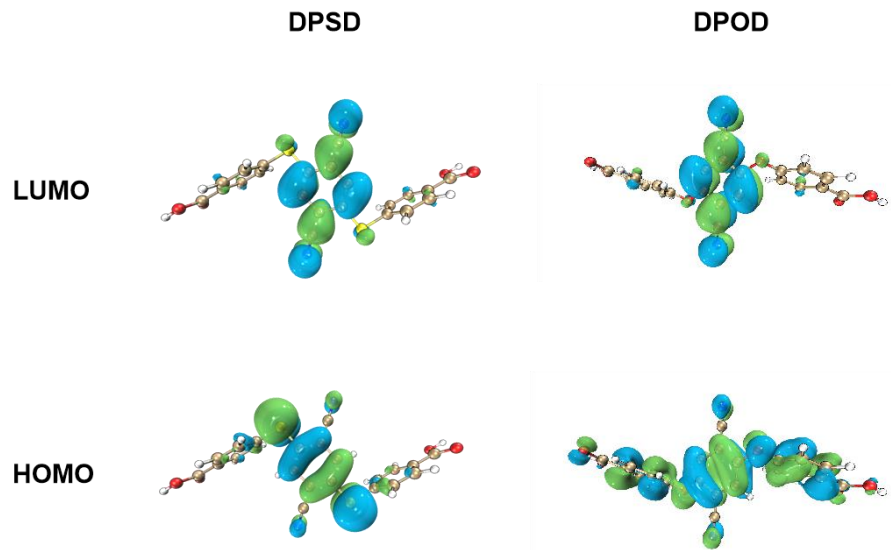


Figure S30. The frontier molecular orbitals (FMOs) of DPSD and DPOD.

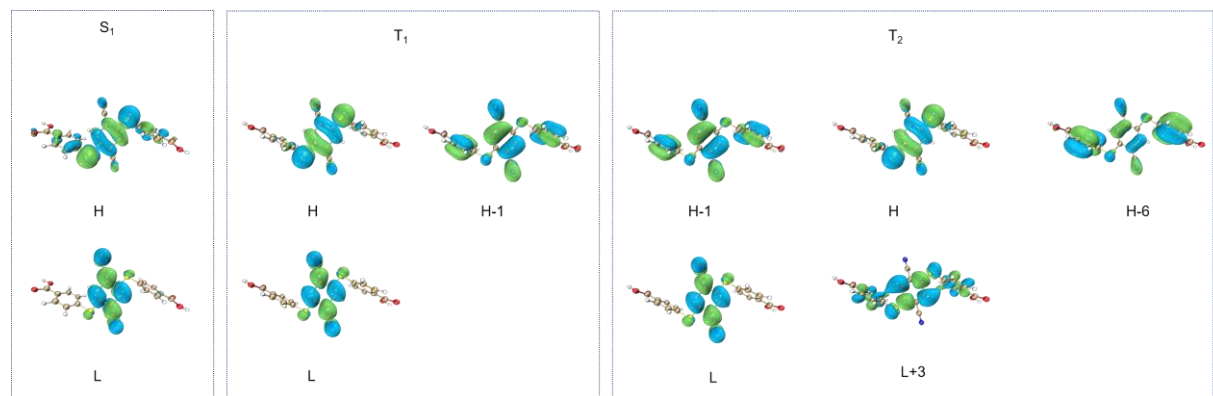


Figure S31. The frontier molecular orbitals (FMOs) in S_1 , T_1 and T_2 for DPSD.

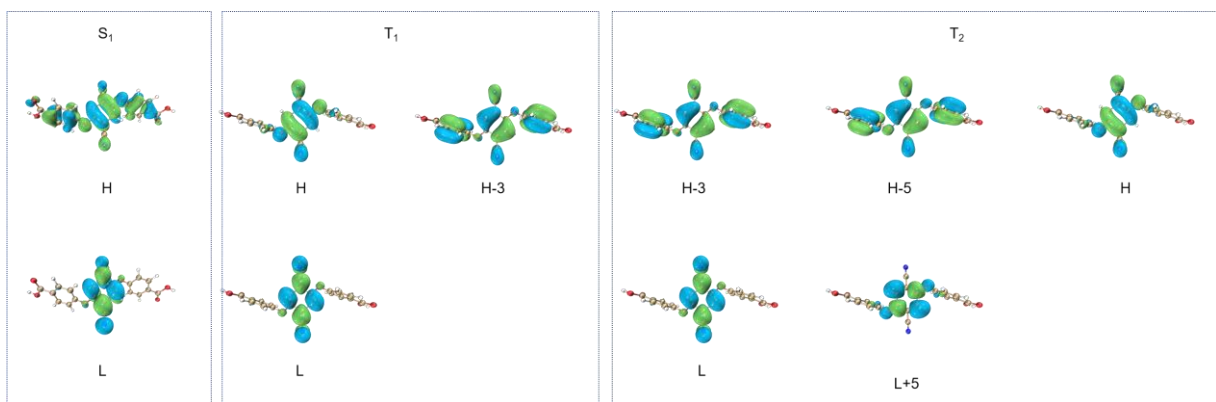


Figure S32. The frontier molecular orbitals (FMOs) in S₁, T₁ and T₂ for **DPOD**.

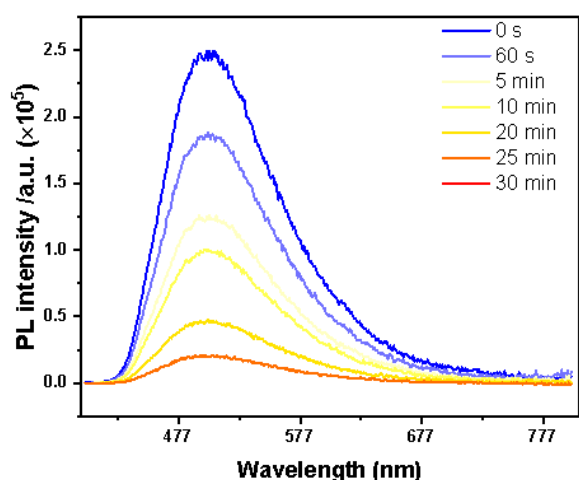


Figure S33. The phosphorescence spectra of **α -Cellulose+DPOD** after water fumigation.

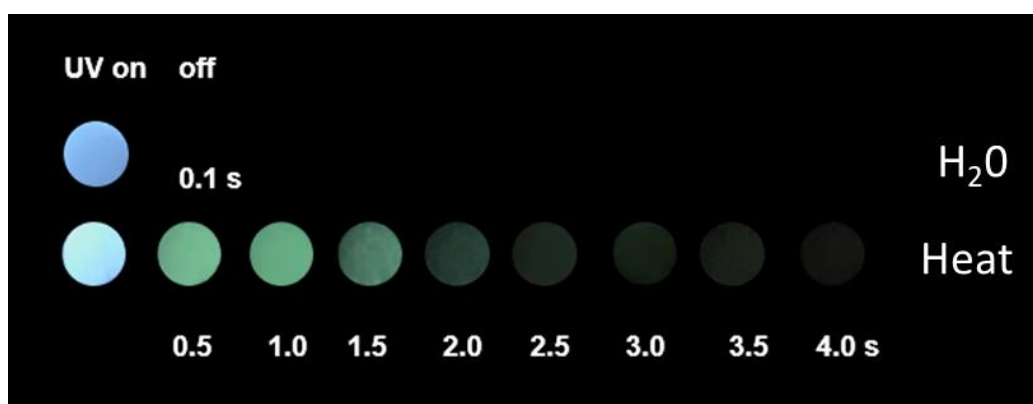


Figure S34. Photographs of the water/heat stimulus-responsive property of **α -Cellulose+DPOD** taken before and after turning off UV-365 nm excitation.

Table S1. Crystal data and structure refinement parameters for **DPSD** and **DPOD**.

Compound	DPSD	DPOD
Empirical formula	C ₂₄ H ₁₅ N ₃ O ₄ S ₂	C ₂₅ H ₁₈ N ₃ O ₇
CCDC NO	2312419	2312421
Formula weight	516.58	472.42
Crystal system	monoclinic	orthorhombic
Space group	<i>P</i> 2 ₁ /c	<i>P</i> bca
a/Å	16.7130(15)	8.5890(5)
b/Å	8.6188(10)	13.1840(8)
c/Å	9.3560(8)	39.0756(17)
$\alpha/^\circ$	90	90
$\beta/^\circ$	103.976(9)	90
$\gamma/^\circ$	90	90
Volume/Å ³	1307.8(2)	4424.9(4)
Z	2	8
$\rho_{\text{calcg}}/\text{cm}^3$	1.312	1.418
μ/mm^{-1}	2.171	0.887
F(000)	536.0	1960.0
Radiation	CuK α ($\lambda=1.54184$)	CuK α ($\lambda=1.54184$)
Data/restraints/parameters	1363/4/172	1380/0/147
GooF	1.116	1.028
R ₂ [I>=2 σ (I)]	R ₁ =0.0471, wR ₂ =0.1245	R ₁ =0.0761, wR ₂ =0.1983
wR ₂ [all data]	R ₁ =0.0535, wR ₂ =0.1310	R ₁ =0.0965, wR ₂ =0.2148

Table S2. The photophysical parameters of host, guest and host+guest at room temperature.

Compounds	α -Cellulose	DPSD	DPOD	α -Cellulose+DPSD	α -Cellulose+DPOD
$\Phi / \%$	6.3	7.3	66.7	7.9	17.6
$\Phi_F / \%$	2.6	7.3	8.5	4.4	7.8
$\Phi_P / \%$	3.7	/	58.2	3.5	9.8
τ_F / ns	3.38	1.52	0.61	3.21	1.47
τ_P / ms	5.60	/	0.00797	11.47	535.21
$K_{ISC} / 10^7 \text{ s}^{-1}$	1.1	/	95.41	1.09	6.67

The photophysical parameters are obtained according to the following equations:^[7]

$$\tau_{F or P} = \tau_1 A_1 + \tau_2 A_2$$

$$K_r^F = \Phi_F / \tau_F$$

$$K_{nr}^F = (1 - \Phi) / \tau_F$$

$$K_r^P = \Phi_P / \tau_P$$

$$K_{nr}^P = (1 - \Phi_P) / \tau_P$$

$$K_{ISC} = (1 - \Phi_F) / \tau_F$$

where F means fluorescence; P means phosphorescence; r means radiative transition; nr means non-radiative transition; ISC means intersystem crossing; τ means average lifetime; K means transition rate.

Table S3. The decay lifetimes of **α -Cellulose** at 440 nm measured at different temperature under the excitation of 340 nm.

Temperature/K	$\tau_1(\text{ns})$	A ₁ (%)	$\tau_2(\text{ns})$	A ₂ (%)	$\tau(\text{ns})$	χ^2
77	2.86	60.60	7.84	39.40	4.82	0.7683
100	2.85	60.60	7.83	39.40	4.81	0.7683
140	2.60	57.56	8.27	42.44	5.01	1.0533
180	2.86	64.90	8.10	35.10	4.70	1.2376
200	2.37	60.49	6.67	39.51	4.07	0.8029
240	1.71	33.74	4.62	66.26	3.64	0.8955
280	2.82	88.15	10.69	11.85	3.75	1.1314
300	1.75	47.81	4.88	52.19	3.38	1.1454

Table S4. The decay lifetimes of **α -Cellulose** at 470 nm measured at different temperature under the excitation of 340 nm.

Temperature/K	τ_1 (ms)	A ₁ (%)	τ_2 (ms)	A ₂ (%)	τ (ms)	χ^2
77	7.20	6.11	241.15	93.89	226.86	1.2835
100	22.92	11.79	245.21	88.21	219.00	1.2279
140	10.0	6.59	228.58	93.41	214.18	1.2672
180	11.76	7.47	227.98	92.53	211.83	1.2887
200	6.14	6.45	149.95	93.55	140.67	1.2392
240	13.07	21.08	128.56	78.92	104.21	0.7082
280	1.46	9.67	40.10	90.33	36.36	1.3306
300	0.49	25.60	7.37	74.40	5.60	1.0567

Table S5. The decay lifetimes of **DPSD** at 455 nm measured at different temperature.

Temperature/K	τ_1 (ns)	A(%)	χ^2
77	4.01	100	1.3303
100	3.81	100	1.2810
140	3.04	100	0.3674
180	2.74	100	0.3305
200	2.37	100	0.3011
240	2.18	100	0.2623
280	1.91	100	0.2243
300	1.52	100	0.5810

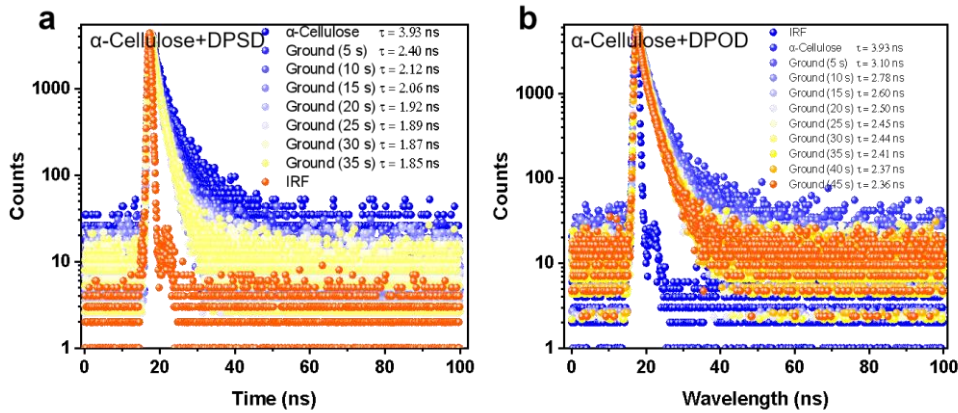
Table S6. The decay lifetimes of **DPSD** at 570 nm measured at different temperature.

Temperature/K	τ_1 (ms)	A ₁ (%)	τ_2 (ms)	A ₂ (%)	τ (ms)	x^2
77	13.27	30.89	65.16	69.11	49.13	1.2318
100	10.03	38.11	54.40	61.89	37.49	1.4399
140	5.82	35.35	37.34	64.65	26.20	1.1690
180	2.97	50.78	22.39	49.22	12.53	0.8494
200	2.03	50.86	17.46	49.14	9.61	0.7568
240	2.00				2.00	0.7412

Table S7. Calculated FRET efficiencies according to the changed fluorescence lifetimes of donor (**α -Cellulose**).

Samples	Ground time (s)	Lifetimes, $\tau_{\alpha\text{-Cellulose}}$ (ns, $e_x=340$ nm, $e_m=440$ nm)	Efficiencies, $E_{\text{FRET}}(\%)$
α-Cellulose	/	3.93	/
	5	2.40	38.93
The mixed sample (α-Cellulose+DPSD)	15	2.06	47.58
	25	1.89	51.91
	35	1.85	52.93

Samples	Ground time (s)	Lifetimes, $\tau_{\alpha\text{-Cellulose}}$ (ns, $e_x=340$ nm, $e_m=440$ nm)	Efficiencies, $E_{\text{FRET}}(\%)$
α-Cellulose	/	3.93	/
	5	3.10	21.12
	15	2.60	33.84
The mixed sample (α-Cellulose+DPOD)	25	2.45	37.66
	35	2.41	38.68
	45	2.36	39.95



The energy transfer efficiencies can be calculated according to the fluorescence lifetimes of donor in the presence and in the absence of acceptor. The FRET efficiency may be estimated based on the equation:^[8-10]

$$E_{\text{FRET}} = 1 - \tau_{\text{DA}} / \tau_{\text{D}}$$

Where τ_{DA} and τ_{D} represent the fluorescence lifetimes of donor in the presence and in the absence of the acceptor, respectively.

Table S8. The decay lifetimes of **α -Cellulose+DPSD** at 470 nm measured at different temperature under the excitation of 340 nm.

Temperature/K	$\tau_1(\text{ns})$	$A_1(\%)$	$\tau_2(\text{ns})$	$A_2(\%)$	$\tau(\text{ns})$	χ^2
77	3.12	35.75	6.85	64.25	5.52	0.9997
100	3.32	42.50	7.06	57.50	5.47	1.0383
140	2.84	30.73	6.24	69.27	5.20	1.0597
180	2.96	39.59	6.31	60.41	4.98	1.0009
200	2.66	39.77	5.88	60.23	4.60	0.8611
240	1.93	27.87	4.89	72.13	4.07	0.8923
280	2.05	41.49	4.52	58.51	3.50	0.9960
300	1.85	48.91	4.51	51.09	3.21	0.8797

Table S9. The decay lifetimes of **α -Cellulose+DPSD** at 554 nm measured at different temperature under the excitation of 340 nm.

Temperature/K	τ_1 (ms)	A ₁ (%)	τ_2 (ms)	A ₂ (%)	τ (ms)	χ^2
77	16.84	23.98	62.90	76.02	51.85	1.0193
100	16.77	26.10	64.01	73.90	51.68	1.2117
140	15.05	28.32	59.89	71.68	47.19	1.3089
180	13.92	30.47	59.87	69.53	45.87	1.2882
200	3.99	9.04	46.02	90.96	42.22	0.8864
240	5.49	23.33	25.25	76.56	20.61	0.8222
280	6.24	26.49	25.95	73.51	20.73	0.8221
300	2.00	42.52	18.48	57.48	11.47	0.8091

Table S10. The decay lifetimes of **DPOD** at 417 nm measured at different temperature.

Temperature/K	τ_1 (ns)	A(%)	χ^2
77	2.39	100	0.7053
100	1.76	100	0.5825
140	1.58	100	0.5029
180	1.08	100	0.3816
200	0.85	100	0.3354
240	0.71	100	0.2736
280	0.69	100	0.2779
300	0.61	100	0.2416

Table S11. The decay lifetimes of **DPOD** at 500 nm measured at different temperature.

Temperature/K	$\tau_1(\mu\text{s})$	A ₁ (%)	$\tau_2(\mu\text{s})$	A ₂ (%)	$\tau(\mu\text{s})$	χ^2
77	2.35	26.99	11.84	73.01	9.28	0.7767
100	2.32	26.49	11.73	73.51	9.24	0.7068
140	2.28	33.40	12.52	66.60	9.10	0.7331
180	2.17	34.65	12.57	65.35	8.97	0.5702
200	2.19	34.91	12.57	65.09	8.95	0.6369
240	2.16	31.63	11.85	68.37	8.79	0.6518
280	2.07	28.91	11.18	71.09	8.55	0.5754
300	1.82	28.04	10.36	71.96	7.97	0.5850

Table S12. The decay lifetimes of **DPOD** at 575 nm measured at different temperature.

Temperature/K	$\tau_1(\text{ms})$	A ₁ (%)	$\tau_2(\text{ms})$	A ₂ (%)	$\tau(\text{ms})$	χ^2
77	59.61	37.45	260.10	62.55	185.02	1.499
100	26.03	16.06	138.20	83.94	120.19	1.453
140	41.83	37.24	140.28	62.76	103.62	1.311
180	5.40	13.82	65.33	86.18	57.05	0.986
200	7.77	15.90	49.24	84.10	42.65	0.907
240	13.86	45.85	39.50	54.15	27.74	0.911
280	6.72	66.36	20.55	33.64	11.37	0.951
300	3.12	79.76	17.16	20.24	5.96	1.047

Table S13. The decay lifetimes of **DPOD** in 2-MTHF (50.0 μM) at 375 nm measured at different temperature.

Temperature/K	$\tau_1(\text{ns})$	A(%)	χ^2
77	1.52	100	0.849
100	1.49	100	0.636
140	1.34	100	0.574
180	1.21	100	0.967
200	1.20	100	0.945
240	1.21	100	0.675
280	1.20	100	0.684
300	1.19	100	0.770

Table S14. The decay lifetimes of **DPOD** in 2-MTHF (50.0 μM) at 486 nm measured at different temperature.

Temperature/K	$\tau_1(\text{ms})$	A ₁ (%)	$\tau_2(\text{ms})$	A ₂ (%)	$\tau(\text{ms})$	χ^2
77	238.53	16.62	849.84	83.38	748.24	1.246
100	39.73	3.0	780.42	97.0	758.20	1.059
140	176.60	11.52	69.34	88.48	81.69	1.219
180	20.28	14.98	48.40	85.02	44.18	1.019
200	0.002	100			0.002	1.112

Table S15. The decay lifetimes of **α -Cellulose+DPOD** at 417 nm measured at different temperature under the excitation of 340 nm.

Temperature/K	τ_1 (ns)	A(%)	χ^2
77	2.38	100	0.5685
100	2.31	100	0.5468
140	2.09	100	0.5534
180	1.96	100	0.5207
200	1.83	100	0.4867
240	1.71	100	0.4227
280	1.55	100	0.4296
300	1.47	100	0.3505

Table S16. The decay lifetimes of **α -Cellulose+DPOD** at 492 nm measured at different temperature under the excitation of 340 nm.

Temperature/K	τ_1 (ms)	A ₁ (%)	τ_2 (ms)	A ₂ (%)	τ (ms)	χ^2
77	254.67	11.42	1142.61	88.58	1041.21	1.1761
100	225.43	23.21	918.95	76.79	757.98	1.1233
140	179.76	19.94	822.02	80.06	693.95	1.2773
180	201.83	22.46	815.05	77.54	677.32	1.1168
200	184.14	21.81	802.53	78.19	667.66	1.1530
240	161.88	19.59	736.97	80.41	624.31	1.0373
280	153.07	19.26	696.68	80.74	591.98	0.7432
300	146.49	21.96	644.59	78.04	535.21	0.8549

Table S17. TD-DFT calculated energy levels of **α -Cellulose+DPSD**.

State	Energy(eV)	Transition configuration
S ₁	2.13	H→L(99.3%)
T ₁	1.80	H→L(91.4%)
T ₂	2.75	H-1→L(94.6%)
T ₃	2.84	H-16→L(46.1%) H-18→L(10.5%) H-9→L(7.1%) H→L(6.6%) H→L+3(6.1%)
T ₄	3.08	H-4→L(81.4%) H-5→L+1(5.8%)
T ₅	3.16	H→L+1(45.2%) H-4→L+1(9.2%) H-4→L+2(6.5%)

Table S18. TD-DFT calculated energy levels of **α -Cellulose+DPOD**.

State	Energy(eV)	Transition configuration
S ₁	2.28	H-1→L(75.2%) H-2→L(24.4%)
T ₁	1.97	H→L+1(81.7%) H-1→L(9.2%)
T ₂	3.12	H-1→L(52.6%) H→L(16.8%) H-16→L(15.5%)
T ₃	3.17	H-1→L(36.2%) H-16→L(35.7%) H-6→L(5.2%)

T ₄	3.49	H-2→L(41.5%) H-6→L+2(24.3%) H→L+2(10.6%) H-7→L+5(6.2%)
T ₅	3.50	H-2→L(50.7%) H-6→L+2(19.5%) H→L+2(9.8%)

Table S19. TD-DFT calculated energy levels of **DPSD**.

State	Energy(eV)	Transition configuration
S ₁	3.29	H→L(95.6%)
T ₁	1.85	H→L (82.2%) H-1→L (11.1%)
T ₂	3.24	H-1→L(48.4%) H→L(16.8%) H→L+3(11.0%) H-6→L(10.5%)
T ₃	3.36	H-4→L+1(32.1%) H-3→L+2(27.2%) H-5→L+5(10.6%) H-6→L+4(10.6%) H-2→L+2(6.4%)
T ₄	3.36	H-4→L+2(31.4%) H-3→L+1(27.7%) H-5→L+4(12.8%) H-6→L+5(8.5%) H-2→L+1(6.5%)
T ₅	3.75	H→L+3(65.4%) H-1→L(15.7%) H→L+5(9.7%)
T ₆	4.16	H→L+1(59.8%) H-2→L+2(10.5%) H-5→L+2(7.2%) H-6→L+1(6.7%)
	4.21	H→L+2(36.7%)

T_7		H-5→L+1(19.2%) H-6→L+2(16.1%) H-2→L+1(11.6%) H-1→L+2(8.6%)
T_8	4.25	H-2→L(63.9%) H-3→L(14.1%) H-14→L(6.2%)
T_9	4.31	H-5→L+2(36.1%) H-6→L+1(29.3%) H→L+1(18.0%) H-1→L+1(7.5%)
T_{10}	4.35	H→L+2(40.5%) H-5→L+1(25.7%) H-6→L+2(18.9%)

Table S20. SOC constants(ξ) between singlet and triplet states of **DPSD**.

Energy levels	SOC constants
$\xi(S_1-T_1)$	0.47 cm ⁻¹
$\xi(S_1-T_2)$	0.10 cm ⁻¹
$\xi(S_1-T_3)$	0 cm ⁻¹
$\xi(S_1-T_4)$	0.95 cm ⁻¹
$\xi(T_1-S_0)$	0 cm ⁻¹

Table S21. TD-DFT calculated energy levels of **DPOD**.

State	Energy(eV)	Transition configuration
S_1	3.69	H→L(91.4%)
T_1	1.83	H→L(91.8%) H-3→L(5.2%)
T_2	3.35	H-3→L(38.3%) H-5→L(35.8%) H→L(9.9%) H→L+5(6.8%)
T_3	3.43	H-1→L+2(33.0%) H-2→L+1(32.7%) H-4→L+4(14.7%) H-3→L+3(8.7%) H-5→L+3(6.4%)

T ₄	3.43	H-1→L+1(32.7%) H-2→L+2(31.5%) H-4→L+3(14.8%) H-3→L+4(8.4%) H-5→L+4(5.7%)
T ₅	4.18	H→L+5(78.6%) H-3→L(6.3%) H-5→L(5.6%)
T ₆	4.54	H-4→L+2(40.9%) H-3→L+1(24.8%) H-5→L+1(15.8%)
T ₇	4.54	H-4→L+1(41.8%) H-3→L+2(24.3%) H-5→L+2(15.6%)
T ₈	4.64	H-4→L+4(28.4%) H-3→L+3(17.1%) H-1→L+2(14.0%) H-2→L+1(13.6%) H-5→L+3(12.2%)
T ₉	4.64	H-4→L+3(31.1%) H-3→L+4(16.9%) H-1→L+1(14.5%) H-2→L+2(13.8%) H-5→L+4(12.0%)
T ₁₀	4.70	H-8→L(62.8%) H→L+10(10.3%) H-13→L(5.8%)

Table S22. SOC constants(ξ) between singlet and triplet states of **DPOD**.

Energy levels	SOC constants
$\xi(S_1-T_1)$	4.32 cm ⁻¹
$\xi(S_1-T_2)$	0.41 cm ⁻¹
$\xi(S_1-T_3)$	0.26 cm ⁻¹
$\xi(S_1-T_4)$	0.91 cm ⁻¹
$\xi(T_1-S_0)$	0.02 cm ⁻¹

REFERENCES

- [1] Dolomanov, O. V.; Bourhis, L. J.; Gildea, R. J.; Howard, J. A. K.; Puschmann, H. OLEX2: a complete structure solution, refinement and analysis program. *J. Appl. Crystallogr.* **2009**, *42*, 339-341.
- [2] Frisch, M. J.; Trucks, G. W.; Schlegel, H. B.; Scuseria, G. E.; Robb, M. A.; Cheeseman, J. R.; Scalmani, G.; Barone, V.; Mennucci, B.; Petersson, G. A.; Nakatsuji, H.; Caricato, M.; Li, X.; Hratchian, H. P.; Izmaylov, A. F.; Bloino, J.; Zheng, G.; Sonnenberg, J. L.; Hada, M.; Ehara, M.; Toyota, K.; Fukuda, R.; Hasegawa, J.; Ishida, M.; Nakajima, T.; Honda, Y.; Kitao, O.; Nakai, H.; Vreven, T.; Montgomery, J. A., Jr.; Peralta, J. E.; Ogliaro, F.; Bearpark, M.; Heyd, J. J.; Brothers, E.; Kudin, K. N.; Staroverov, V. N.; Kobayashi, R.; Normand, J.; Rahavachari, K.; Rendell, A.; Burant, J. C.; Iyengar, S. S.; Tomasi, J.; Cossi, M.; Rega, N.; Millam, J. M.; Klene, M.; Knox, J. E.; Cross, J. B.; Bakken, V.; Adamo, C.; Jaramillo, Gomperts, R.; Stratmann, R. E.; Yazyev, O.; Austin, A. J.; Cammi, R.; Pomelli, C.; Ochterski, J. W.; Martin, R. L.; Morokuma, K.; Zakrzewski, V. G.; Voth, G. A.; Salvador, P.; Dannenberg, J. J.; Dapprich, S.; Daniels, A. D.; Farkas, O.; Foresman, J. B.; Ortiz, J. V.; Cioslowski, J.; Fox, D. J. Gaussian, Inc. Wallingford CT, 2009.
- [3] Lu, T.; Chen, F. Multiwfn: a multifunctional wavefunction analyzer. *J. Comput. Chem.* **2012**, *33*, 580-592.
- [4] Lu, T.; Chen, Q. Interaction Region Indicator: A Simple Real Space Function Clearly Revealing Both Chemical Bonds and Weak Interactions**. *Chemistry—Methods* **2021**, *1*, 231-239.
- [5] Humphrey, W.; Dalke, A.; Schulten, K. VMD: Visual Molecular Dynamics. *J. Mol. Graphics* **1996**, *14*, 33-38.
- [6] Riebe, S.; Vallet, C.; van der Vight, F.; Gonzalez-Abradelo, D.; Wölper, C.; Strassert, C. A.; Jansen, G.; Knauer, S.; Voskuhl, J. Aromatic Thioethers as Novel Luminophores with Aggregation-Induced Fluorescence and Phosphorescence. *Chem. Eur. J.* **2017**, *23*, 13660-13668.
- [7] Bi, X.; Shi, Y.; Peng, T.; Yue, S.; Wang, F.; Zheng, L.; Cao, Q. E. Multi-Stimuli Responsive and Multicolor Adjustable Pure Organic Room Temperature Fluorescence-Phosphorescent Dual-Emission Materials. *Adv. Funct. Mater.* **2021**, *31*, 2101312.
- [8] Wang, K.; Gao, Z.; Zhang, W.; Yan, Y.; Song, H.; Liu, X.; Zhou, Z.; Meng, H.; Xia, A.; Yao, J. Exciton funneling in light-harvesting organic semiconductor microcrystals for wavelength-tunable lasers. *Sci. Advance.* **2019**, *6*, eaaw2953.
- [9] Baronas, P., Kreiza, G., Mamada, M., Maedera, S., Adoménas, P., Adoménienė, O., Kazlauskas, K., Adachi, C., and Juršėnas, S. Enhanced energy transfer in doped bifluorene single crystals: prospects for organic lasers. *Adv. Opt. Mater.* **2020**, *8*, 1901670.
- [10] Wang, B., Yu, Y., Zhang, H., Xuan, Y., Chen, G., Ma, W., Li, J., and Yu, J. Carbon dots in a matrix: energy-transfer-enhanced room-temperature red phosphorescence. *Angew. Chem., Int. Ed.* **2019**, *58*, 18443- 18448.